

## Optical and Electrical Properties and Band Structure of GeTe and SnTe\*

R. TSU, W. E. HOWARD, AND L. ESAKI

*IBM Watson Research Center, Yorktown Heights, New York 10598*

(Received 22 March 1968)

We describe first our measurements of the variation with carrier concentration of the susceptibility mass and the absorption edge, in a range of hole concentrations of  $1 \times 10^{20}$  to  $2 \times 10^{21}$   $\text{cm}^{-3}$ . The susceptibility mass for holes varies from 0.075 to  $0.51m_0$  for the lowest and highest carrier concentrations, respectively. These properties, and similar published data for SnTe, together with the Fermi energies and energy gaps obtained from tunneling experiments, have been interpreted using a band structure obtained by applying the  $\mathbf{k} \cdot \mathbf{p}$  perturbation approach at the  $L$  point of a face-centered cubic zone. We have assumed a coupling scheme such that there is strong transverse coupling across the energy gap while the longitudinal coupling is between the principal conduction band and the second valence band. The energy separations for the second valence bands required in both materials are 0.5 and 0.34 eV for GeTe and SnTe, respectively. As a prerequisite to a meaningful interpretation of the measured quantities versus carrier concentration, we have calculated the ratio of the actual carrier concentration to the Hall concentration  $1/R_{0e}$ . We have made numerous computer calculations and have obtained a set of band parameters for these materials based on the best fit for a wide variety of experimental results.

### I. INTRODUCTION

SOME initial measurements of the optical and electrical properties of single-crystal GeTe have been reported by the authors<sup>1</sup> for fairly high hole concentrations ( $10^{21}$   $\text{cm}^{-3}$ ). In the present work, we have extended these measurements to lower carrier concentrations, using thin films evaporated onto heated NaCl substrates.

One of the principal results of these experiments is that the susceptibility mass shows a pronounced dependence upon carrier concentration, characteristic of narrow gap semiconductors. In particular, the results are rather similar to those of Dixon and Riedl<sup>2</sup> for PbTe and Riedl *et al.*<sup>3</sup> for SnTe. For both GeTe<sup>4</sup> and SnTe<sup>5,6</sup> there is evidence of a second valence band being occupied for large carrier concentrations. An interesting feature of the GeTe data is that the variation susceptibility mass with carrier concentrations in the two-band region is opposite to that observed for SnTe. For GeTe, the mass increases more rapidly with concentration when two bands are occupied, while for SnTe, the mass increases less rapidly in the two-band region.

We have interpreted these results using an approach similar to that used by Dixon and Riedl<sup>2</sup> for PbTe, with some important differences. First, we used a four-band model (two conduction bands and two valence bands) with the particular coupling scheme proposed

for PbTe by Dimmock and Wright.<sup>7</sup> The principal feature of their coupling scheme is that the  $\mathbf{k} \cdot \mathbf{p}$  coupling across the principal energy gap is transverse only. The validity of this model for lead salts has been challenged by the work of Lin and Kleinman<sup>8</sup>; nevertheless, as we shall show, it does give good agreement with experiments for the cases of GeTe and SnTe, for a particular combination of band parameters. Second, it is known that for the nonellipsoidal energy surfaces which result from such an approach, it is essential that the Hall coefficient be calculated as a function of the actual carrier concentration. Allgaier<sup>9</sup> has calculated the ratio of the Hall concentration,  $N_H = 1/R_{0e}$ , to the actual carrier concentration for SnTe using a constant relaxation time. His results yield too large a variation with carrier concentration relative to experiment.<sup>10</sup> We have found that by the use of a constant mean free path, and the incorporation of a second valence band, the agreement with experiment is much improved.

Since both the tunneling results of Stiles *et al.*<sup>11</sup> and the present concentration dependence of susceptibility mass suggest a small energy gap approximately 0.1–0.2 eV for GeTe, we assume that the observed optical absorption edges for our films at 0.7–1.0 eV are strongly Burstein-shifted. Accordingly, we use the measured absorption edges primarily to obtain approximate Fermi energies for the films, by comparing with calculated shapes of the absorption edge for various Fermi energies.

\* Sponsored in part by the U. S. Army Research Office, Durham, N.C., under Contract No. DA 31-124-ARO-D-478.

<sup>1</sup> R. Tsu, W. E. Howard, and L. Esaki, *Solid State Commun.* **5**, 167 (1967).

<sup>2</sup> J. R. Dixon and H. R. Riedl, *Phys. Rev.* **138**, A873 (1965).

<sup>3</sup> H. R. Riedl, J. R. Dixon, and R. B. Schoolar, *Phys. Rev.* **162**, 692 (1967).

<sup>4</sup> N. V. Kolomoets, E. Ya. Lev, and L. M. Sysoeva, *Fiz. Tverd. Tela* **6**, 706 (1964) [English transl.: *Soviet Phys.—Solid State* **6**, 551 (1964)].

<sup>5</sup> R. F. Brebrick and A. J. Strauss, *Phys. Rev.* **134**, 104 (1964).

<sup>6</sup> J. R. Burke, R. S. Allgaier, B. B. Houston, J. Babiskin, and

P. G. Siebenmann, *Phys. Rev. Letters*, **14**, 360 (1965).

<sup>7</sup> J. O. Dimmock and G. B. Wright, *Phys. Rev.* **135**, A821 (1964).

<sup>8</sup> P. J. Lin and L. Kleinman, *Phys. Rev.* **142**, 478 (1966).

<sup>9</sup> B. B. Houston, R. S. Allgaier, J. Babiskin, and P. G. Siebenmann, *Bull. Am. Phys. Soc.* **9**, 80 (1964).

<sup>10</sup> R. S. Allgaier, *Phys. Rev.* **152**, 808 (1966).

<sup>11</sup> P. J. Stiles, L. Esaki, and W. E. Howard, in *Proceedings of the Tenth International Conference on Low-Temperature Physics, Moscow, 1966* (Proizvodstvenno-Izdatel'skii Kombinat, VINITI, Moscow, 1967); L. Esaki, *J. Phys. Soc. Japan Suppl.* **21**, 589 (1966).

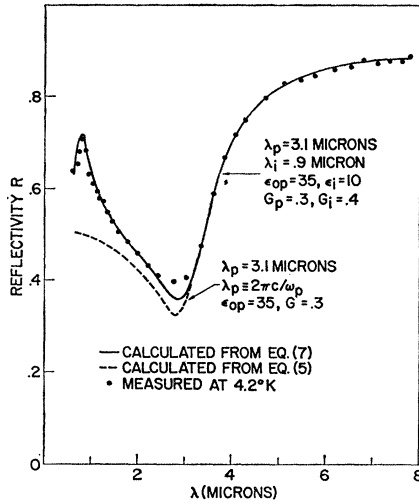


FIG. 1. Reflectivity versus wavelength for the single-crystal bulk GeTe fitted to two dispersion relations.

The best sets of band parameters for GeTe and SnTe which provide the good agreement with experiment mentioned above were obtained by comparing numerous computer calculations of the susceptibility masses, Fermi energies, etc., based on our four-band model, with those values measured, or available. The Shubnikov-de Haas results<sup>6,12</sup> for SnTe have been used to check the band parameters. This procedure gives us added confidence in the determined band parameters. We feel that using fcc symmetry for GeTe is a good approximation for our purposes, and the results seem to justify this position. On the other hand, our results would not apply for very low carrier concentrations where the properties would be expected to be more sensitive to the discrepancy between fcc symmetry and the actual symmetry of GeTe, which is fcr (face-centered rhombohedral).

## II. EXPERIMENTAL RESULTS FOR GeTe

### A. Preparation of Samples

We evaporated GeTe films using both the molecular-beam and the electron-beam techniques, on the (100) surfaces of the heated NaCl substrates. All substrates are carefully polished. In general, the electron beam evaporation gives us more uniform films. Best results are obtained for an evaporation rate of a few hundred angstrom units of film thickness per minute. In Table I, those samples designated by the letter *E* were prepared by electron beam evaporation. The samples with asterisks are highly polycrystalline, while the other films show (111) preferred orientations by x-ray spectroscopy. Generally speaking, higher substrate temperature results in lower carrier concentration.

<sup>12</sup> J. R. Burke, B. Houston, H. J. Savage, J. Babiskin, and P. G. Siebenmann, J. Phys. Soc. Japan Suppl. 21, 384 (1966).

TABLE I.  $N_H$  and  $\mu_H$  at 2.95, 77, and 4.2°K for the samples evaporated at the substrate temperatures as shown.

Sample	Substrate $T$ (°C)	$T=295^\circ\text{K}$		$T=77^\circ\text{K}$		$T=4.2^\circ\text{K}$	
		$N_H=1/R_0e$ ( $10^{20}\text{ cm}^{-3}$ )	$\mu_H$	$N_H$	$\mu_H$	$N_H$	$\mu_H$
284E	305	1.47	180	1.27	573	1.27	800
271E	305	1.5	177	1.46	495		
270E	290	1.57	120				
455	300	2.25	126	1.95	267	1.87	348
3b	300	2.75	135	2.34	280	2.29	465
1a	290	2.58	120				
3a	290	2.67	132	2.67	276		
2a*	290	3.4	60	3.5	108		
454*	260	5.22	36				
2b*	250	6.3	23	5.85	68	5.85	75
383E*	150	11.5	20	11.5			
Single crystal		21.4	36	21.2	60	21.2	110

However, for substrate temperature greater than 310°C, nucleation begins to be unpredictable, and one may get no films.

### B. Dispersion Relation for Photons

In order to clarify the precise relationship for a non-parabolic band structure between the plasma frequency obtained in reflectivity measurements and the band parameters, we shall review briefly the dispersion relation for photons. The classical dispersion relation for photons polarized in a given direction, say, the  $x$  direction, in a medium represented by a dielectric constant  $\epsilon_{op}$  and a conductivity  $\sigma_x$ , is

$$q^2 c^2 / \omega^2 = \epsilon_{op} (1 - 4\pi\sigma_x / i\omega\epsilon_{op}), \quad (1)$$

where  $q$  and  $\omega$  are the wave number and frequency of the photons. The conductivity derived from the first-order iteration of the classical Boltzmann transport equation, neglecting the spatial variation, may be written as

$$\sigma_x = \frac{e^2}{i\omega\hbar} \frac{1}{4\pi^3} \int dV_k \frac{(\partial E / \partial k_x)(\partial f_0 / \partial k_x)}{1 - i\omega\tau}, \quad (2)$$

in which  $f_0$  is the distribution function,  $E$  the energy of the carriers,  $k_x$  the  $x$  component of the momentum,  $\tau$  the velocity-dependent relaxation time, and  $dV_k$  the differential volume element in  $\mathbf{k}$  space. For  $\omega\tau \gg 1$ , the integrand of the imaginary part of  $\sigma_x$  is independent of  $\tau$ ; thus it is customary to define

$$\frac{4\pi \text{Im}\sigma_x}{\omega\epsilon_{op}} \equiv \frac{\omega_p^2}{\omega^2}, \quad (3)$$

where  $\omega_p$  is the well-known plasma frequency, and by analogy with the free-electron plasma, to define also a susceptibility mass  $m_s$  by

$$m_s = 4\pi N e^2 / \epsilon_{op} \omega_p^2, \quad (3')$$

where  $N$  is the total carrier concentration and  $\omega_p = 2\pi c / \lambda_p$ . Because these materials are highly degenerate, we

TABLE II. The optical dielectric constants  $\epsilon_{op}$ , the plasma wavelengths  $\lambda_p$ , and the empirical susceptibility masses  $m^* \equiv m_s/r$  for the GeTe samples measured at 205, 77, and 4.2°K.

$N_H$ at 77°K ( $10^{20}$ cm $^{-3}$ )	$T=295^\circ\text{K}$			$T=77, 4.2^\circ\text{K}$		
	$\epsilon_{op}$	$\lambda_p(\mu)$	$m^*/m_0$	$\epsilon_{op}$	$\lambda_p(\mu)$	$m^*/m_0$
1.27	36	5.58	0.098	34	5.22	0.092
1.46	40	5.60	0.103			
1.57	37.4	5.45	0.112			
1.95	36.5	5.27	0.134	35	5.1	0.13
2.34	37	5.0	0.142	35	4.7	0.132
2.58	36.3	5.07	0.162	35.4	4.75	0.147
2.67	34	4.55	0.144	33	4.3	0.134
3.5	36	4.6	0.184	34.5	4.25	0.164
5.22	37	4.47	0.25			
5.85	38	4.25	0.249	34	3.85	0.226
11.5	37.5	3.55	0.35	35	3.45	0.348
21.2	37.5	3.15	0.5	35	3.1	0.51

have used the Fermi distribution function at zero temperature for  $f_0$ . Writing  $dV_k = dSdE/|\nabla_k E|$ , there results from Eqs. (2) and (3) the ratio of  $N$  to  $m_s$  in terms of a surface integral over the Fermi surface, i.e.,

$$\frac{N}{m_s} = \sum_j \frac{1}{3\hbar} \times \frac{1}{4\pi^3} \int_{E_F} v dS, \quad (4)$$

in which  $v$  is the magnitude of the velocity defined by  $v = (1/\hbar)|\nabla_k E|$ ,  $E_F$  is the Fermi energy, and  $j$  is the band index. If the plasma frequency can be measured, one may calculate  $N/m_s$  from Eq. (3'). Meanwhile, if the energy dispersion  $E(\mathbf{k})$  is known for the carriers, we may calculate  $N/m_s$  from Eq. (4). Therefore Eqs. (3'), (3), and (4) form the link between the measured plasma frequency and the energy dispersion  $E(\mathbf{k})$ . From Eq. (2), we note that for  $\omega\tau \sim 1$ ,  $\text{Im}\sigma_x$ , like  $\text{Re}\sigma_x$ , will be dependent on frequency in a complicated way because  $\tau$  is not a constant. However, Eq. (2) is essentially the classical Drude model, which is only a fair approximation. As long as  $\tau$  is strictly a constant, or  $\omega\tau \gg 1$ , which is almost the case at low temperatures for all our samples, we can rewrite Eq. (1) in the usual form

$$\frac{q^2 c^2}{\omega^2} = (n + ik)^2 = \epsilon_{op} \left[ 1 - \frac{1}{(\omega/\omega_p)^2 + i(\omega/\omega_p)G_p} \right], \quad (5)$$

in which  $n$ ,  $k$ , and  $G_p$  are the refractive index, the extinction coefficient, and  $1/\omega_p\tau$ , respectively. The reflectivity is defined in terms of  $n$  and  $k$  by

$$R = \frac{(n-1)^2 + k^2}{(n+1)^2 + k^2}. \quad (6)$$

The determination of  $\lambda_p$  for GeTe single crystals from the measured reflectivity, using Eqs. (5) and (6), has been previously reported.<sup>1</sup> However, for wavelengths near the interband transition, additional absorption processes give rise to much higher reflectivity. If we approximate the interband processes by a harmonic oscillator term at a frequency  $\omega_i$ , and a damping con-

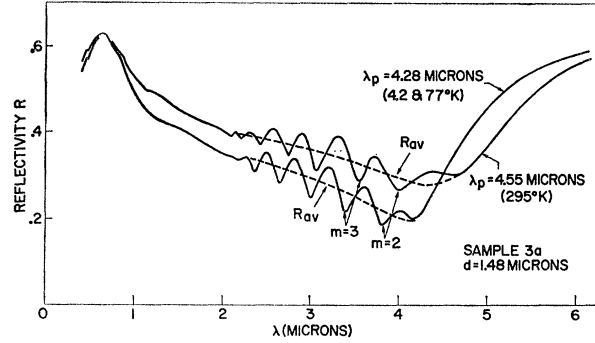


FIG. 2. Measured reflectivity for film 3a at 295, 77, and 4.2°K.

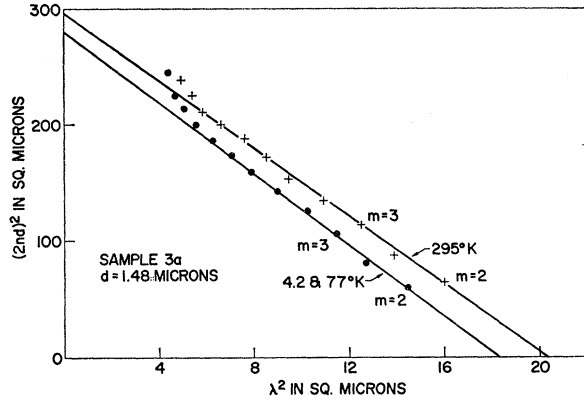
stant  $G_i$ , the dispersion law becomes

$$(n + ik)^2 = \epsilon_i - \frac{\epsilon_{op} - \epsilon_i}{(\omega/\omega_i)^2 - 1 + i(\omega/\omega_i)G_i} - \frac{\epsilon_{op}}{(\omega/\omega_p)^2 + i(\omega/\omega_p)G_p}, \quad (7)$$

in which  $\epsilon_i$  defines a dielectric constant in the region where interband processes are important. In order to verify the previous determinations of  $\omega_p$  for use herein, we have refitted Fig. 1 of Ref. 1 using Eqs. (6) and (7). Figure 1 shows the results of curve fitting. With the exception of obtaining new parameters  $\epsilon_i$ ,  $\omega_i$ , and  $G_i$ , the other parameters, namely,  $\epsilon_{op}$ ,  $\omega_p$ , and  $G_p$ , are unchanged. As long as  $\omega_p$  and  $\omega_i$  are not too close to each other, it is easy to distinguish the plasma dispersion from the interband dispersion. In view of the fact that all our present work involves lower carrier concentrations, and thus lower plasma frequencies, we have chosen to use the simple dispersion law of Eq. (5) as our model for the study of the optical properties of GeTe. Previously, we have pointed out<sup>1</sup> that the use of interference fringes for the determination of  $\epsilon_{op}$  and  $\omega_p$  requires, in the case of GeTe, that the losses be taken into account. While this is strictly true even for the lower carrier concentrations considered here, the error introduced by ignoring losses and using a straight-line fit of  $(nd)^2$  versus  $\lambda^2$  is only a few percent in the present case. Since this is acceptable, we have chosen to use the simple straight-line fit for the present analysis of our data.

### C. Optical and Electrical Measurements

Table I shows the results of Hall measurements giving the Hall mobility and  $N_H \equiv 1/R_{0e}$  at 295, 77, and 4.2°K. Note that those samples evaporated at higher temperatures have lower carrier concentrations and higher mobilities. Table II shows the results of a simple straight-line fit of the interference fringes for the reflectivity in films, as discussed previously. Note that  $m^*$  is not the same as the definition of susceptibility

FIG. 3.  $(2nd)^2$  versus  $\lambda^2$  for film 3a.

mass  $m_s$  defined by Eqs. (3') and (5). In order to express the ratio  $N/m_s$  in terms of the measured concentration  $N_H \equiv N/r$ , we define  $m^* \equiv m_s/r = (4\pi N_H e^2) / \epsilon_{op} \omega_p^2$ , which is the quantity used in Table II. Then

$$N/m_s = N_H/m^*, \quad (8)$$

and we have a basis for comparing theory with experiment. Alternatively, one can calculate  $r$  (as we describe in Sec. III) and convert  $m^*$  to  $m_s$ .

Figure 2 shows a typical example of the measured reflectivity. Figure 3 shows the corresponding plot of  $(2nd)^2$  versus  $\lambda^2$ . The intercept of the straight line with the ordinate gives  $(2nd)^2$  at  $\lambda=0$ , i.e.,  $\epsilon_{op}$ ; the intercept with the abscissa gives  $\lambda_p^2$ . For this sample at 295°K,  $\lambda_p$  is 4.55  $\mu$ , and the minimum in reflectivity of the smoothed reflectivity,  $R_{av}$ , occurs around 4.37  $\mu$ . Riedl *et al.*<sup>3</sup> only fit  $R_{av}$  to the computed reflectivity because of the difficulty of measuring film thickness on cleaved substrates. Their method requires a relatively thick film.

In determining the absorption coefficient  $\alpha$ , defined by  $\alpha = 4\pi k/\lambda$ , we use

$$T = \frac{(1-R_1)(1-R_2)(1-R_3)\exp(-\alpha d)}{(1-R_2R_3)[1-(R_1R_2+R_1R_3(1-R_2)^2)\exp(-2\alpha d)]}, \quad (9)$$

where  $R_1$  and  $R_2$  are the reflectivities of the film-air and film-substrate interfaces, and  $R_3$  is the reflectivity of the substrate. We have found that two films from a single evaporation, prepared side by side on a substrate, may be different, because the temperature of the substrate and the evaporation rates are very critical. This is why we have not used a method involving two films of different thicknesses. A typical absorption curve versus photon energy is shown in Fig. 4. Note that the edge is relatively steep and that the apparent energy gap is greater than 0.6 eV. Other samples show similar edges; however, they are shifted slightly in energy, according to their carrier concentrations. The

samples with higher carrier concentrations have edges shifted to higher energies generally, with the total spread being 0.3 eV. Absorption coefficients less than about  $10^4 \text{ cm}^{-1}$  have not been observed because of free carrier absorption, which is apparent in the low-energy portion of the curve. The absorption curve is shifted towards the lower energy region at 295°K as compared to that at 4.2°K. This is consistent with the measurements of the energy gap by tunneling spectroscopy<sup>10</sup> showing a decrease in energy gap at 295°K.

### III. BAND MODELS FOR GeTe AND SnTe

The Shubnikov-de Haas results<sup>6,12</sup> for SnTe, which has fcc symmetry, show that its principal valence band consists of multiple (111) extrema. GeTe, of course, has fcr symmetry. However, it is nearly cubic, so we assume that to a first approximation it may be treated as cubic, with the same fourfold degeneracy in energy bands as SnTe. It is well known that for PbTe, the conduction- and valence-band extrema are both at the (111) zone boundary; therefore, one is led to try for GeTe and SnTe a band structure similar to that of the lead salts. Specifically, Dimmock and Wright proposed as a basis for a band structure of the lead salts an ordering of bands at the  $L$  point as shown in Fig. 5. This ordering leads to a plane-wave coupling scheme as indicated on the right-hand side of the figure, in their notation. The double-headed arrows indicated allowed  $\mathbf{k} \cdot \mathbf{p}$  coupling for transverse and longitudinal directions. As mentioned in the Introduction, this scheme may not, in fact, be valid for the lead salts. Lin and Kleinman,<sup>8</sup> for example, cite evidence that the valence band state should be  $L_6^+(L_1)$  rather than  $L_{4,5}^+(L_3)$ . Furthermore, there is some evidence that longitudinal as well as transverse coupling across the energy gap is important in PbTe. This fact is attributed by Lin and Kleinman to the spin-orbit mixing in the plane-wave representation. Cuff *et al.*<sup>13</sup> arrived at almost the same ordering scheme as Lin and Kleinman in their comparison of experiment with theory for the lead salts. At any rate, this question is of secondary interest as

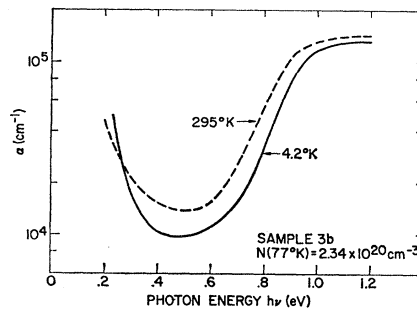


FIG. 4. Absorption coefficient versus photon energy.

<sup>13</sup> K. F. Cuff, M. R. Ellett, C. D. Kuglin, and L. R. Williams, in *Proceedings of the Seventh International Conference on the Physics of Semiconductors: Radiation Damage in Semiconductors* (Dunod Cie., Paris, 1964), p. 677.

far as GeTe and SnTe are concerned. We have used a four-band model with the coupling scheme of Dimmock and Wright, as shown in Fig. 5. As for the other selection rules of Fig. 5, shown with dashed arrows, it will be apparent that while the comparison with experiment leads to no contradictions in this regard, neither is it very sensitive to mixing and coupling with more remote bands. Therefore, the band shown in Fig. 5 as  $E_{c2}$  is dashed. It should be clear from our approach that we used only the coupling scheme as shown in Fig.

5; the specific labelling of the bands is not important. For instance, there might well be spin-orbit mixing of the bands in the  $\mathbf{k}\cdot\mathbf{p}$  representation.

In all of our experiments, there exists no evidence of a second conduction band  $E_{c2}$  lying near the other bands. Thus we assume that  $E_{\Delta c}$  is large in comparison to  $E_g$  and  $E_{\Delta v}$ . As a result, we may approximate the  $4\times 4$  secular determinant of the  $\mathbf{k}\cdot\mathbf{p}$  representation by a  $3\times 3$  determinant involving only the two valence bands and the principal conduction band, which is

$$\begin{vmatrix} E_g + \frac{\hbar^2 k_l^2}{2m_0} - E' & \hbar k_l P_l / m_0 & \hbar k_l P_l / m_0 \\ \hbar k_l P_l / m_0 & -\frac{\hbar^2 k_l^2}{2m_l(v1)} - E' & 0 \\ \hbar k_l P_l / m_0 & 0 & E_g - E_{\Delta v} + \frac{\hbar^2 k_l^2}{2m_0} \end{vmatrix} = 0, \quad (10)$$

$$\left\{ \begin{array}{l} E_g - E_{\Delta v} + \frac{\hbar^2 k_l^2}{2m_0} \\ -\frac{\hbar^2 k_l^2}{2m_0} \left[ \frac{m_0}{m_l(v2)} - 1 \right] - E' \end{array} \right\}$$

where  $E' = E - \hbar^2 k_l^2 / 2m_0$ . The notations  $m_l(v1)$  and  $m_l(v2)$  denote the longitudinal and the transverse masses of the first and second valence bands, respectively. Moreover, if  $\hbar^2 k_{lF}^2 / 2m_l(c1)E_{\Delta v} < 1$ , where  $k_{lF}$  is the longitudinal Fermi momentum and  $m_l(c1)$  is the approximate equivalent parabolic longitudinal mass of the first conduction band, we may further reduce Eq. (10) to a  $2\times 2$  determinant involving only the principal conduction and valence bands, together with an approximate parabolic second valence band. Because both GeTe and SnTe are  $p$  type, we shall give only the solution pertinent for the valence band,

$$E_{v1}(\mathbf{k}) = \frac{1}{2}E_g + \frac{1}{4}\hbar^2 k_l^2 \left( \frac{1}{m_l(c1)} - \frac{1}{m_l(v1)} \right) + \frac{\hbar^2 k_l^2}{2m_0} - \frac{1}{2} \left\{ \left[ E_g + \frac{1}{2}\hbar^2 k_l^2 \left( \frac{1}{m_l(c1)} + \frac{1}{m_l(v1)} \right) \right]^2 + 4\hbar^2 k_l^2 P_l^2 / m_0^2 \right\}^{1/2}. \quad (11)$$

The energy dispersion  $E_{v1}$  is parabolic with respect to  $k_l$  for small  $k_l$  and essentially linear with respect to  $k_l$  for small  $k_l$ . The energy dispersion for the second valence band may be approximated by

$$E_{v2}(\mathbf{k}) = E_g - E_{\Delta v} - \frac{\hbar^2 k_l^2}{2m_l(v2)} - \frac{\hbar^2 k_l^2}{2m_l(v2)}, \quad (12)$$

where

$$m_0 / m_l(v2) = m_0 / m_l(c1) - 2. \quad (13)$$

Using a set of band parameters given by Table III for these materials based on the best fit for a wide variety of experimental results, we found that the ratio  $\hbar^2 k_{lF}^2 / 2m_l(c1)E_{\Delta v} \approx 1.0$  and 2 for GeTe and SnTe, respectively. This shows that within the region of interest the first longitudinal conduction band and the second longitudinal valence bands are very close to parabolic for GeTe. We have made some calculations based on the full three-by-three determinant in view of the fact that the above-mentioned ratio is bigger than unity for SnTe. Results show that the parabolic approximation is adequate for the calculation of such quantities as the Fermi energy and the susceptibility mass, which are within a few percent of the corresponding quantities for the exact model. On the other hand, the use of the exact energy dispersion greatly complicates the calculation of the Hall coefficient. For this reason, we have used the approximate solution represented by Eqs. (11) and (12) for all subsequent computations.

## IV. CALCULATIONS

### A. Calculation of $N/N_H$ from $E(\mathbf{k})$

As pointed out earlier, the measured quantities are not  $N$  and  $m_s$ , but rather  $N_H$  and  $m^*$ , as shown by Eq. (8). Furthermore, all the other measured quantities including the Shubnikov-de Haas data were given in terms of  $N_H$ . Therefore, in order to compare with experimental data for the determination of our band parameters  $E_g$ ,  $E_{\Delta v}$ ,  $m_l(v1)$ ,  $m_l(c1)$ ,  $P_l$ ,  $m_l(v2)$ , and  $m_l(v2)$ , we need to calculate the ratio  $r = N/N_H$ .

TABLE III. The best set of band parameters for our band model for GeTe and SnTe. SnTe\* indicates the band parameters determined for the third-order determinantal solution for the energy dispersion relation.

	$E_g$ (eV)	$E_{\Delta_0}$ (eV)	$\frac{P_i^2}{m_0}$ (eV)	$\frac{P^2}{m_0}$ (eV)	$\frac{m_l(v1)}{m_0}$	$\frac{m_l(c1)}{m_0}$	$\frac{m_l(v2)}{m_0}$	$\frac{m_l(v2)}{m_0}$
GeTe	0.1	0.60	6.8	0.34	0.85	0.425	2.8	2.8
SnTe	0.2	0.54	6.5		0.28	0.07	0.07	0.033
SnTe*	0.2	0.54	6.5	2.92	0.28			0.03

In view of the fact that Allgaier<sup>9</sup> has calculated in detail the ratio  $r = N/N_H = NR_0e$ , we shall only give our results for velocity-dependent relaxation time. For the benefit of the reader, we shall make a few brief remarks about the steps taken for such a derivation. Usually we refer to the laboratory coordinate space for the components of the fields and currents in a Hall measurement. However, the current

$$J = \frac{e^2}{4\pi^3} \int v_i f dV_k \quad (14)$$

involves an integration in  $k$  space. Thus we may utilize the symmetry properties in  $k$  space. Transforming the components of the electric and magnetic fields from the cubic system to the eight (111) coordinate systems of the reciprocal lattice, we solve for the currents in the (111) systems with inversion symmetry and rotational symmetry about the (111) axes. Using the second-order iterative solution of the Boltzmann transport equation, without the spatial and temporal parts,<sup>14</sup> we obtained the ratio

$$r = Ne\alpha'/\sigma_0^2, \quad (15)$$

with

$$\sigma_0 = -\frac{e^2}{3\pi^3} \int \frac{\partial f_0}{\partial E} dV_k \tau v^2 \quad (16a)$$

and

$$\alpha' = \frac{4}{3}(b_{32} + 2b_{21} - a_{11} - a_{33} - \bar{a}_{33}), \quad (16b)$$

in which

$$\begin{aligned} a_{33} &= \frac{e^3}{4\pi^3 \hbar} \int \frac{\partial f_0}{\partial E} dV_k \tau^2 v_1^2 v_{3,3}, \\ \bar{a}_{33} &= \frac{e^3}{4\pi^3 \hbar} \int \frac{\partial f_0}{\partial E} dV_k \tau^2 v_2^2 v_{3,3}, \\ a_{11} &= \frac{e^3}{4\pi^3 \hbar} \int \frac{\partial f_0}{\partial E} dV_k \tau^2 v_2^2 v_{1,1}, \\ b_{21} &= \frac{e^3}{4\pi^3 \hbar} \int \frac{\partial f_0}{\partial E} dV_k \tau^2 v_1 v_2 v_{2,1}, \\ b_{32} &= \frac{e^3}{4\pi^3 \hbar} \int \frac{\partial f_0}{\partial E} dV_k \tau^2 v_2 v_3 v_{3,2}, \end{aligned} \quad (17)$$

where  $v_{i,j} \equiv \partial v_i / \partial k_j$ .

<sup>14</sup> R. A. Smith, *Wave Mechanics of Crystalline Solids* (John Wiley & Sons, Inc., New York, 1961), p. 330.

We have calculated  $r$  using  $E_{v1}$ , by numerical method for both GeTe and SnTe using a velocity-dependent relaxation time  $\tau = 1/avN_{sc} = l/v$ , where  $a$  is the scattering cross section,  $l$  is the mean free path, and  $N_{sc}$  is the density of scatterers. This relaxation time has been shown by Kanai *et al.*<sup>15</sup> to be applicable to the lead salts where the major scattering of carriers is due to neutral defects; including, presumably, highly screened charged centers. Specifically, he assumes that  $N_{sc} = N$ . We have found for SnTe that the calculated  $r$  for constant  $l$  is much closer to the measured than that for constant relaxation time. It is important to note that "constant" mean free path refers to a given carrier concentration. Samples having different carrier concentrations might be expected to have different values for  $l$ ; for example, the variation of mobility given in Table I can be shown to be approximately consistent with Kanai's assumption that  $N_{sc} = N$ , so that  $l$  varies as  $N^{-1}$ .

Because  $\alpha'$  and  $\sigma_0^2$  both involve  $l^2$ ,  $r$  does not depend on  $l$  as long as  $l$  is not a function of  $v$ . Although we do not have the measured value for  $r$  in the case of GeTe, we found that the use of such a constant mean free path is essential in order to fit the measured variation of the susceptibility mass with concentration.

For the second valence band  $E_{v2}$  of Eq. (12), we may integrate  $\sigma_0$  and  $\alpha'$  in closed form, giving

$$\begin{aligned} \sigma_0 &= (8e^2 l / 3\pi^2 \hbar^3) m_l(v2) E_f J / 2\sqrt{\beta}, \\ \alpha' &= (2e^3 l^2 / 3\pi^2 \hbar^2) (1+I) k_m, \end{aligned} \quad (18)$$

where

$$\begin{aligned} J &= 1/\sqrt{\beta} + \sin^{-1}(1-1/\beta)^{1/2} / (1-1/\beta)^{1/2}, & \beta > 1 \\ &= 1/\sqrt{\beta} + [1/(1-\beta)^{1/2}] \ln[1 + (1-\beta)^{1/2} / \\ & \quad 1 - (1-\beta)^{1/2}], & \beta < 1 \end{aligned}$$

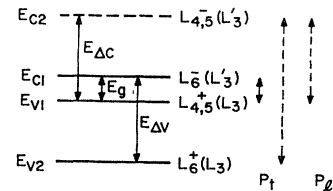


FIG. 5. A schematic representation of the energy-band states at the  $L$  point showing the coupling scheme appropriate for GeTe and SnTe. The longitudinal and transverse matrix elements are denoted by  $P_l$  and  $P_t$ , respectively.

<sup>15</sup> Y. Kanai, R. Nii, and N. Watanabe, *J. Appl. Phys. Suppl.* **32**, 2146 (1961).

$$\begin{aligned}
 I &= k_m \int_0^{k_m} \frac{dk_i}{k_m^2 \beta + (1-\beta)k_i^2} \\
 &= \frac{1}{2(\beta^2 - \beta)^{1/2}} \ln \frac{\beta + (\beta^2 - \beta)^{1/2}}{\beta - (\beta^2 - \beta)^{1/2}}, \quad \beta > 1 \\
 &= \frac{1}{(\beta - \beta^2)^{1/2}} \tan^{-1} [(\beta - \beta^2)/\beta^2]^{1/2}, \quad \beta < 1
 \end{aligned}
 \tag{19}$$

in which  $k_m^2 = 2m_i(v2)E_f/\hbar^2$  and  $\beta = m_i(v2)/m_i(v2)$ . The concentration  $N$  for the paraboloidal band is  $4k_m^3/3\pi^2\beta$ , giving

$$r_2 = 2(1+I)/J^2. \tag{20}$$

Taking both bands into account, we may calculate  $r$  as a function of carrier concentration from

$$r = (N_1 + N_2) \left/ \frac{(\sigma_{o1} + \sigma_{o2})^2}{(\alpha_1' + \alpha_2')} \right., \tag{21}$$

where the subscripts 1 and 2 represent the principal and the subsidiary valence bands.

**B. Calculation of the Absorption Coefficient  $\alpha$**

The absorption coefficient for an allowed direct transition between the principal valence band and the principal conduction band can be written as<sup>16</sup>

$$\alpha = \frac{2\pi e^2 \hbar P_i^2}{3n c m_0^2 \hbar v 4\pi^3} \int d\mathbf{k} \delta(\hbar v - E_{c1} + E_{v1}), \tag{22}$$

where  $P_i$  is the momentum matrix element assumed to be constant and  $n$  is the refractive index. This becomes a surface integral over the surface  $S(\mathbf{k})$  defined by

$$\hbar v - E_{c1}(\mathbf{k}) + E_{v1}(\mathbf{k}) = 0, \tag{23}$$

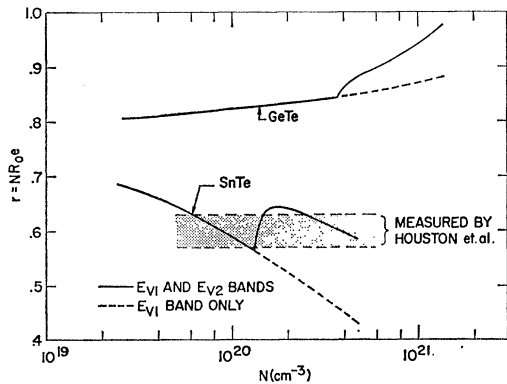


FIG. 6. Hall ratio  $r = NR_0e$  versus carrier concentration  $N$ , for GeTe and SnTe, calculated using the  $\mathbf{k}\cdot\mathbf{p}$  model and the "best fit" parameters given in Table III. The dashed curves represent the single-valence-band results. The shaded region defines the experimental results of Houston *et al.* (see Ref. 9).

<sup>16</sup> H. Y. Fan, Rept. Progr. Phys. 19, 107 (1956).

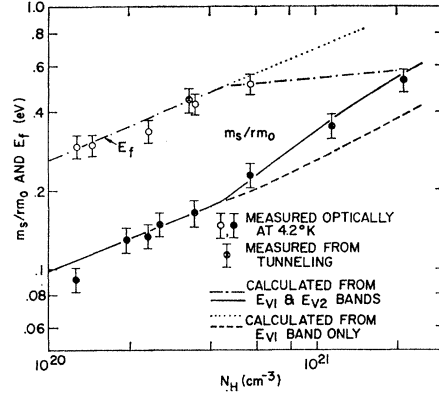


FIG. 7. GeTe: Empirical susceptibility mass  $m^* \equiv m_s/rm_0$  and Fermi energy versus Hall concentration  $N_H = 1/R_0e$ . Experimental masses are from Table II and Fermi energies are from absorption-edge fits and tunneling. The curves are calculated using the  $\mathbf{k}\cdot\mathbf{p}$  model.

so that

$$\alpha(\hbar v) = \frac{e^2 P_i^2}{6\pi^2 n c m_0^2 v} \int_S \frac{dS}{|\nabla_k(\hbar v)|}. \tag{24}$$

This integral may be computed numerically for the surfaces  $E_{c1}$  and  $E_{v1}$  described previously. When  $E_f$  is not negligible, the integral over initial states at 0°K must exclude those for which  $|E_{v1}| < |E_f|$ .

**V. COMPARISON WITH EXPERIMENTAL RESULTS**

We shall list the experimental data used to obtain the band parameters for GeTe and SnTe.

For GeTe, we use (1) the results of Table II for the susceptibility mass versus carrier concentration; (2) the absorption edges for the same samples; and (3) the Fermi energy and energy gap obtained from tunneling for  $N_H \approx 3.2 \times 10^{20} \text{ cm}^{-3}$ .

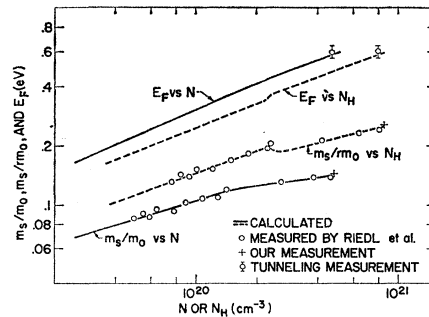


FIG. 8. SnTe: Empirical susceptibility mass  $m^* \equiv m_s/rm_0$  and Fermi energy versus Hall concentration  $N_H$  (dashed curves). Susceptibility mass  $m_s$  and Fermi energy versus carrier concentration  $N$  (solid curves). Experimental masses are from Riedl *et al.* (see Ref. 3) and from a measurement by the authors, while the Fermi energy is from tunneling. The curves are calculated using the  $\mathbf{k}\cdot\mathbf{p}$  model.

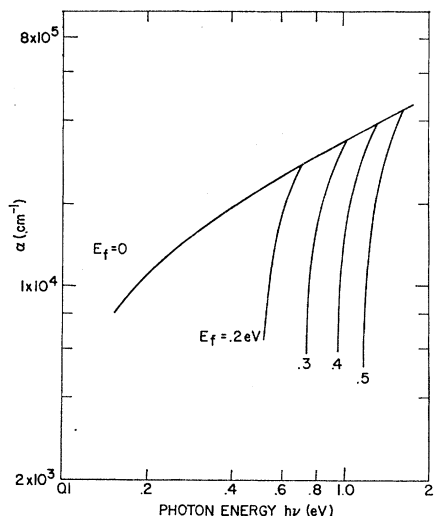


Fig. 9. Calculated absorption coefficient for various Fermi energies showing the Burstein-shifted absorption edges.

For SnTe, we use (1) the variation of susceptibility mass with carrier concentration, as measured by Riedl *et al.*<sup>3</sup>; (2) the Fermi energy and energy gap determined from tunneling<sup>11</sup> for  $N_H \approx 8 \times 10^{20} \text{ cm}^{-3}$ ; (3) the Shubnikov-de Haas data of Burke *et al.*<sup>6,12</sup> for several carrier concentrations; and (4) the relationship between Hall constant and carrier concentration determined by Houston *et al.*<sup>9</sup> over a wide range of carrier concentrations.

The best set of band parameters obtained for GeTe and SnTe are tabulated in Table III. In the process of picking these parameters, we have made numerous calculations with the help of a computer. Figure 6 shows the calculated  $r$  as a function of concentration  $N$  for GeTe and SnTe using the band parameters obtained. The reported experimental range for SnTe is shown by the shaded region. The dashed lines apply to a single valence band  $E_{v1}$ . The discontinuity is due to the onset of carrier occupation of the second band  $E_{v2}$ . Note that the calculated  $r$  for SnTe is in good agreement with the experimental results.<sup>9</sup> This agreement depends heavily on the choice of small  $m_l(c1)$  as compared to  $m_l(v1)$ . Figure 7 shows the comparison of measured  $m^*$  with those calculated as a function of  $N_H$ . In Fig. 8 we have shown both  $m_s$  versus  $N$  and  $m_s/r$  versus  $N_H$  for comparison. The experimental data for  $m_s/r$  versus  $N_H$  were obtained by taking the values of Riedl *et al.* divided by 0.6, because their susceptibility mass  $m_s(\text{Riedl}) = 0.6m^*$ , and their concentration  $N(\text{Riedl}) = 0.6N_H$ . The sharp turn in  $m^*$  versus  $N_H$  becomes quite gradual in the  $m_s$ -versus- $N$  plot.

The computed absorption for the case of GeTe is shown in Fig. 9 for several values of  $E_f$ . This figure clearly demonstrates the Burstein shift, but in addition, it shows the effect on a shifted absorption edge of the difference in longitudinal masses for the two bands.

For  $m_l(c1) = m_l(v1)$ , the absorption rises vertically to the unshifted,  $E_f = 0$ , absorption. A mismatch of masses produces a broader rise, as shown for GeTe. We associate the steep rise of the observed absorption with the steep portion of the calculated absorption edge, particularly since the observed absorption at the top of the steep rise is only about a factor of 2 higher than the calculated. Figure 10 shows a comparison of observed and calculated. Since the discrepancy in magnitude of absorption is relatively minor, we have chosen to determine Fermi energies by shifting vertically the observed and calculated curves to obtain a best over-all fit to one of the family of Burstein-shifted absorption edges. The Fermi energy used to generate that curve is then taken as the Fermi energy for the particular sample under consideration. Since the degree of vertical shift affects the value of the Fermi energy so deduced, the bars on the Fermi-energy points of Fig. 7 reflects primarily an estimate of the limits of error of this procedure.

The band-edge energy dispersion relations for GeTe and SnTe are shown in Fig. 11. The use of our particular coupling scheme makes  $m_l(v2) = m_l(c2)$ . Since we have no information which bears directly on the value of  $E_{\Delta c}$ , the  $E_{c2}$  bands are shown dashed.

For the magnetic field parallel to the 111 axis, we have calculated the minimum frequency of Shubnikov-de Haas oscillation at  $N_H = 1.3 \times 10^{20} \text{ cm}^{-3}$  to be  $9.7 \times 10^5 \text{ G}$ . This value compares favorably with the first two lowest frequencies measured by Burke *et al.*<sup>12</sup> in the [111] direction, namely, being  $8.2 \times 10^5$  and

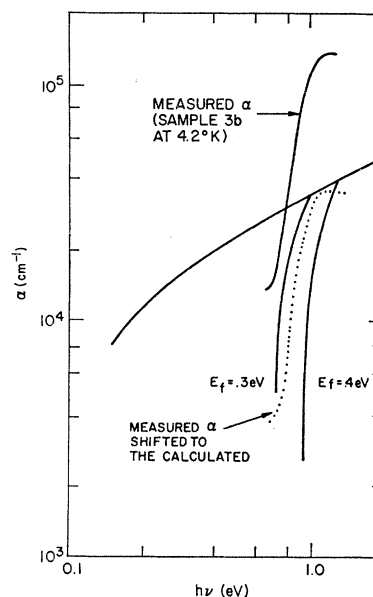


Fig. 10. A typical measured absorption edge for GeTe, compared to absorption calculated for several Fermi energies, using the  $\mathbf{k} \cdot \mathbf{p}$  band model and the best-fit parameters given in the text. The measured absorption is shown shifted vertically as done in the determination of Fermi energy for the sample.

$10 \times 10^5$  G. A reason for taking the average of these has been given by Stiles and Esaki.<sup>17</sup> Basically, they suggested the existence of a phase transition of SnTe from fcc to fcr at a temperature above the temperature of the Shubnikov-de Haas measurements. The lifting of the fourfold degeneracy due to this transition both increases and decreases the minimum frequencies. The calculated frequency at  $N_H = 5 \times 10^{20} \text{ cm}^{-3}$  is  $7.0 \times 10^5$  G, which is a little higher than the measured, being  $6.7 \times 10^5$  G. A separate paper<sup>18</sup> is being prepared to apply our model to the complete Shubnikov-de Haas data for all angles of the applied magnetic field with respect to the various axes. We feel quite confident that the second band is also located at the  $L$  point of the Brillouin zone for SnTe. For GeTe, it is possible that the second band may be associated with another point such as the  $\Sigma$  point. That is to say that the second valence band at the  $L$  point assumed in the four-band scheme might be relatively close in energy, but still low enough that it will never be occupied.

We have shown the energy surfaces  $E_{v1}(\mathbf{k})$  for SnTe in Fig. 12. Note that the surface is slightly dumbbell shaped. The energy surface for GeTe is a mildly distorted ellipsoid. This is because  $m_i(c1)$  for GeTe is much larger than that for SnTe. The dashed curves show the exact energy surfaces using Eq. (10). The discrepancy between the exact energy surface to our approximated surface is not important as far as the computations for  $E_f$ ,  $m_s$ , etc., are concerned; however, it may be important in the calculation of the Shub-

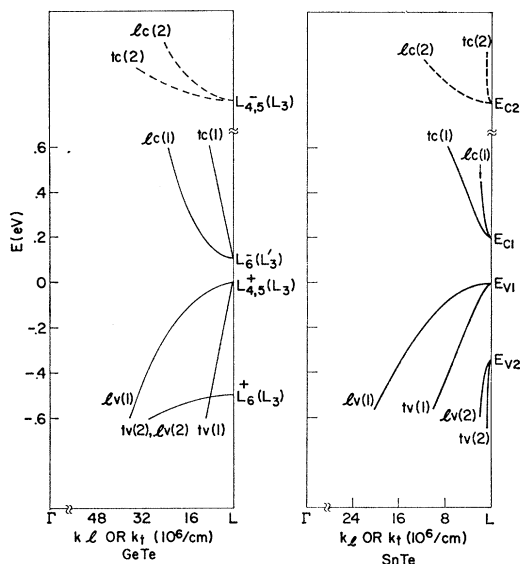


FIG. 11.  $E$  versus  $k$  curves for GeTe and SnTe corresponding to the best-fit set of parameters given in Table III. The labeling of the bands is intended simply to show the correspondence to the model of Dimmock and Wright for PbTe (see Ref. 7).

<sup>17</sup> P. J. Stiles and L. Esaki, recorded comments following contribution by Burke *et al.* (Ref. 11).

<sup>18</sup> P. J. Stiles, W. E. Howard, and R. Tsu (unpublished).

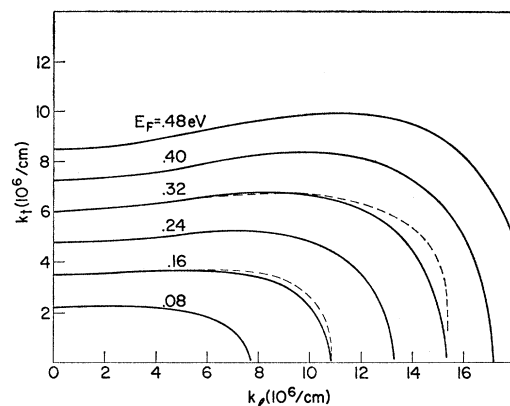


FIG. 12. Section of the calculated Fermi surfaces for SnTe. The dashed curves represent the use of the full secular determinant of Eq. (10).

nikov-de Haas cross section as a function of orientation of applied magnetic field.

## VI. SUMMARY

We wish to emphasize several points: (1) The values of  $E_g$  at low temperature used to fit the experimental results are small, i.e., 0.1 and 0.2 eV for GeTe and SnTe, respectively; this confirms roughly the small energy gaps, 0.2 and 0.3 eV, determined from tunneling. (2) The ability to fit the qualitatively different variations of susceptibility mass in the two-band region can be associated with both the smaller mass for the second valence band in SnTe, as compared to GeTe, and with the assumption of constant mean free path for carriers. (3) In the case of SnTe, the small value of  $m_i(c1)$  which equals  $m_i(v2)$  in the simple coupling scheme is not only acceptable, but definitely improves the fit to experiment relative to, say,  $m_i(c1) = m_i(v1)$ . As mentioned earlier, this small value of  $m_i(c1)$  is also important to the agreement of the Hall coefficient with experiment. (4) In the case of GeTe, the relatively poorer agreement at lower carrier concentrations may be caused by lifting of the fourfold degeneracy for the fcr symmetry, since the cubic approximation would be expected to be quite poor in the limit of low carrier concentrations. (5) Although the determined band parameters are not unique, we found that the range of variation from the set of parameters given are not great, being  $\pm 5\%$ . For instance, we can decrease  $m_s$  by increasing  $m_i(v1)$ , then bring back  $m_s$  by decreasing  $P_t$ . However, this process would also reduce  $E_f$ . (6) The calculation of the ratio between the actual carrier concentration to  $N_H$  for such a nonellipsoidal energy surface is an important addition to the understanding of the measured quantities for GeTe and SnTe. (7) The differences in anisotropy for the conduction and valence bands in GeTe and SnTe produce a broadening of the Burstein-shifted absorption edges. Using a simple four-

band model for GeTe and SnTe, assuming that the most significant couplings between bands are a transverse momentum coupling between the principal valence and conduction bands and a longitudinal coupling between the principal conduction and the second valence bands, we are able to explain most of the available experimental results for GeTe and SnTe.

#### ACKNOWLEDGMENTS

We are grateful to P. J. Stiles for his many helpful suggestions, D. O'Kane for supplying us the single-crystal GeTe and SnTe, J. Angilello for the x-ray work, and T. Hajos and J. Cummings for part of the optical and galvanomagnetic measurements.

### Optical Properties of VO<sub>2</sub> between 0.25 and 5 eV

HANS W. VERLEUR, A. S. BARKER, JR., AND C. N. BERGLUND

*Bell Telephone Laboratories, Murray Hill, New Jersey 07971*

(Received 5 April 1968)

The optical constants of VO<sub>2</sub> have been determined between 0.25 and 5 eV both below and above the semiconductor-metal transition temperature  $T_t=340^\circ\text{K}$ . Reflectivity and transmission spectra have been measured on both single crystals and thin films. The reflectivity spectra of the bulk crystals were measured with  $\mathbf{E}\perp$  ( $c$  axis) in the tetragonal phase [or  $\perp$  ( $a$  axis) in the monoclinic phase], and with  $\mathbf{E}$  parallel to these axes. While there are some differences in magnitude between the dielectric constants obtained from thin-film and single-crystal measurements, the structural features are in good agreement. Below  $T_t$  there are four prominent absorption peaks centered near photon energies of 0.85, 1.3, 2.8, and 3.6 eV. Above  $T_t$ , metallic free-carrier absorption is observed below 2.0 eV, but the same two absorption peaks near 3 and 4 eV are present. The energy location and polarization dependence of these two higher energy peaks can be related to similar absorption peaks in rutile, and are interpreted using the rutile band structure. The results are consistent with a picture in which filled bands arising primarily from oxygen  $2p$  orbitals are separated by approximately 2.5 eV from partially filled bands arising primarily from vanadium  $3d$  orbitals. Transitions from the filled  $2p$  bands are responsible for the high-energy peaks in the optical absorption in both the high- and low-temperature phases. In the high-temperature metallic phase, there is evidence that there is overlap among the  $3d$  bands such that at least two bands are partially occupied by the extra  $d$  electron per vanadium ion. In the low-temperature semiconductor phase, a band gap of approximately 0.6 eV opens up within the  $3d$  bands, separating two filled bands from higher-lying empty bands. The two absorption peaks at 0.85 and 1.3 eV are due to transitions from these two filled bands.

#### 1. INTRODUCTION

IT has been shown that VO<sub>2</sub> is one of several transition-metal oxides which show an abrupt change in some physical property such as electrical resistance or magnetic susceptibility at a temperature  $T_t$ .<sup>1,2</sup> In VO<sub>2</sub> the transition is probably best described as a first-order semiconductor-to-metal transition accompanied by a lattice distortion with  $T_t=68^\circ\text{C}$ . While no theory has yet been developed which predicts the transition temperature in VO<sub>2</sub>, recent work with idealized models pictures the transition as being of electronic origin.<sup>2,3</sup> The models suggest that above  $T_t$  the extra  $3d$  electron derived from each V<sup>4+</sup> ion resides in a partially filled  $d$  band giving metallic conduction. As the temperature is lowered it becomes energetically favorable for the crystal structure to change from tetragonal to monoclinic and for an energy gap to appear. Thus, below  $T_t$  VO<sub>2</sub> has a distorted structure, with a filled band separated by a gap from an empty band.

In this paper the optical properties of VO<sub>2</sub> are studied in the range 0.25 to 5.0 eV. In an earlier study,<sup>1</sup> to be referred to as I, the infrared phonon and free-electron dispersion properties were measured above and below the transition temperature  $T_t\approx 68^\circ\text{C}$ . The present work extends the spectra to investigate the electron-band transitions both above and below  $T_t$ . In I, it was found that bulk single-crystal VO<sub>2</sub> samples exhibited infrared-active phonon modes for  $T < T_t$  in the energy range  $\hbar\omega = 0.02$  to 0.09 eV. When samples were heated above  $T_t$ , the infrared spectra showed a sudden increase in reflectivity which was fit satisfactorily by assuming the appearance of  $\sim 2 \times 10^{21}$  quasifree electrons per cc. The large dielectric function of these carriers obscured the phonon peaks preventing any infrared optical study of the phonons in the high temperature phase. This large free carrier part of the dielectric function  $\epsilon$  extended up to energies of about 2.0 eV. In the present study which includes bulk crystals and thin-film measurements, free carriers dominate the spectra (for  $T > T_t$ ) below 2.0 eV. However, there is significant structure in the absorption both above and below  $T_t$  at photon energies above 2.5 eV, and additional peaks near 1.0 eV for

<sup>1</sup> A. S. Barker, Jr., H. W. Verleur, and H. J. Guggenheim, *Phys. Rev. Letters* **17**, 1286 (1966).

<sup>2</sup> David Adler and Harvey Brooks, *Phys. Rev.* **155**, 826 (1967).

<sup>3</sup> G. J. Hyland, *J. Phys. C* **1**, 189 (1968).